Mechanistic study of a low-power bacterial maintenance state using high-throughput electrochemistry

John A. Ciemniecki[1], Chia-Lun Ho[2,4], Richard D. Horak[1], Akihiro Okamoto[2,3,4,5]*, Dianne K. Newman[1,6*]

[1] Division of Biology & Biological Engineering, California Institute of Technology, Pasadena CA 91125

[2] Research Center for Macromolecules and Biomaterials, National Institute for Materials Science, 1-1 Namiki, Tsukuba, Ibaraki 305-0044, Japan

[3] Faculty of Life and Environmental Sciences, University of Tsukuba, 1-1-1 Tennodai, Tsukuba Ibaraki 305-8577, Japan

[4] School of Chemical Sciences and Engineering, Hokkaido University, 13 Kita, 8 Nishi, Kita-ku, Sapporo, Hokkaido 060-8628, Japan.

[5] Living Systems Materialogy (LiSM) Research Group, International Research Frontiers Initiative (IRFI), Tokyo Institute of Technology, Yokohama, Kanagawa 226-8501, 669 Japan.

[6] Division of Geological & Planetary Sciences, California Institute of Technology, Pasadena CA 91125

*co-corresponding authors: dkn@caltech.edu, okamoto.akihiro@nims.go.jp

SUMMARY

Mechanistic studies of life's lower metabolic limits have been limited due to a paucity of tractable experimental systems. Here we show that redox-cycling of phenazine-1-carboxamide (PCN) by *Pseudomonas aeruginosa* supports cellular maintenance in the absence of growth with a low mass-specific metabolic rate of 8.7 x 10^{-4} W (g C)$^{-1}$ at 25˚C. Leveraging a high-throughput electrochemical culturing device, we find that non-growing cells cycling PCN tolerate conventional antibiotics but are susceptible to those that target membrane components. Under these conditions, cells conserve energy via a noncanonical, facilitated fermentation that is dependent on acetate kinase and NADH dehydrogenases. Across PCN concentrations that limit cell survival, the cell-specific metabolic rate is constant, indicating the cells are operating near their bioenergetic limit. This quantitative platform opens the door to further mechanistic investigations of maintenance, a physiological state that underpins microbial survival in nature and disease.

INTRODUCTION

The physiology of bacteria in non- or slowly-growing states is poorly understood relative to its ubiquity in natural, clinical, and engineered systems[1,2]. A fundamental question underlying the study of this state is how much energy is needed to maintain cell viability in the absence of growth[3]. Previous laboratory attempts to quantify this value inferred maintenance metabolic rates by extrapolating the energy needed to support zero growth from values measured during slow growth in continuous culture[4]. Yet these estimates are consistently two to four orders of magnitude higher than metabolic rates measured in stable natural environments where sources of energy or nutrients are limiting[5]. How can we bridge the gap between the two to study the cellular strategies underpinning non-growth maintenance metabolism?

While environmental measurements inspire an interest in this attenuated energetic state, it is important to note that metabolic rates estimated from environmental samples, by necessity, also rest on inferences rather than direct measurements. First, it is assumed that all the cells counted in the sample are metabolically active. Second, the fraction of cells using the measured nutrient is often estimated using educated guesses. Third, it is unclear which percentage of cells are in a normal vs. viable-but-non-culturable (VBNC) state with a diminished metabolism[6]. Overestimates of any of these parameters can inflate the relevant cell count, leading to underestimates of the cell-specific metabolic rate. Accordingly, the development of laboratory systems in which to study metabolic rates at or near zero growth coupled to measurements of single-cell metabolic activity is needed[7]. While progress is being made towards defining new systems through which to understand the biology of growth arrest[8–10], to our knowledge, no high-throughput experimental systems have been established that permit direct measurements of metabolic power output during this state.

A powerful motivation for doing so comes from the fact that non-growing cells inhabit the cores of biofilms, multicellular aggregates found in many chronic infections. Most antibiotics used in the clinic fail to eradicate biofilms, contributing to the deaths of millions of people annually[11,12]. Cells within biofilms tolerate many conventional drugs[11], and tolerance can beget antibiotic resistance[13]. The mechanisms driving this tolerance are complex[14–17]; biofilm-associated metabolic changes are one important factor. The ability of diverse biofilm-forming bacteria to withstand standard antibiotics is not surprising because screens for novel antibiotics have mainly been performed using growth-based assays[18] and most antibiotics target the cellular processes that sustain actively growing cells, such as cell wall synthesis, translation, and DNA replication. While conventional antibiotics are highly effective at inhibiting or killing fast-growing bacterial

pathogens that have not acquired resistance, the ability of biofilm bacteria to tolerate their presence remains an unsolved and medically important challenge[11]. Quite simply, we struggle to eradicate cells that exist in attenuated metabolic states because we do not have a mechanistic understanding of maintenance physiology due to a scarcity of tractable experimental systems.

We hypothesized that anaerobic extracellular electron transfer (EET) could be leveraged to measure the metabolic flux powering maintenance (*i.e*. the minimum energy needed to support cellular integrity and preserve a culturable state in the absence of growth) and investigate its bioenergetic underpinnings. *Pseudomonas aeruginosa*, an opportunistic pathogen and model biofilm-forming organism, produces phenazines ($C_{12}H_8N_2R$, e.g. Figure 1B right), a widespread class of colorful, heterocyclic, redox-active metabolites[19]. Phenazines promote biofilm development and attenuated metabolism (sometimes referred to as "dormancy") in biofilm regions where oxygen is unavailable, rendering cells physiologically tolerant to conventional drugs[20,21]. Previously, using low-throughput electrochemical reactors, we showed that the phenazines pyocyanin, phenazine-1-carboxylic acid and 1-hydroxy phenazine act as extracellular electron shuttles that facilitate an anaerobic survival metabolism[22], one that supports survival but not growth of the bulk population. While *P. aeruginosa* cannot survive anaerobically via glucose fermentation[23], when provided with phenazines and a re-oxidizing potential, intracellular redox-balance is achieved, permitting glucose catabolism and substrate-level phosphorylation (SLP) via the AckA-Pta pathway[24] (Figure 1B). In this way, ATP is generated via a noncanonical form of energy conservation where reduction of the extracellular electron shuttle facilitates SLP and organic acid excretion[24], similar to energy conservation strategies found in other bacteria in the presence of humic substances or flavins[25–29]. Given this fermentative energy conservation pathway requires redox-balancing using an exogenous oxidant, we refer to it as a *facilitated fermentation* (Figure 1A). Because it supports survival without growth, we reasoned that the rate of this facilitated fermentation may reveal the metabolic flux necessary for cell maintenance under these conditions.

In this study, we investigated phenazine EET survival metabolism using a recently developed high-throughput electrochemical system that enables nearly 100 measurements of current generated by planktonic cultures to be measured concurrently[30]. By leveraging this system to survey a wide range of conditions and directly measure power output, we asked: What is the metabolic rate of phenazine EET-mediated survival and how does it compare to the basal metabolic rates measured for other organisms across the tree of life? At the single-cell level, are cells surviving without growth in a maintenance state or is the population surviving via a balance of growth and death? Which types of antibiotics can kill cells in this physiological state? Which

enzymes contribute to its catabolism? And does phenazine EET power cell survival at or above the maintenance power requirement? Broadly, our results introduce a tractable experimental platform that permits quantitative and mechanistic investigations into maintenance physiology. More specifically, they shed light on the minimal metabolic requirements and pathways that contribute to powering *P. aeruginosa* cells under anoxic conditions relevant to the antibiotic tolerant core of biofilms.

RESULTS

To study phenazine-dependent survival metabolism at the lowest thermodynamic potential possible for the metabolism, we performed our studies using phenazine-1-carboxamide (PCN), the phenazine derivative with the lowest standard midpoint potential (-140 mV E°', [31]) of those produced in significant quantities by *P. aeruginosa*[32,33]. Due to its low potential, PCN reduction should permit EET-based survival metabolism with the smallest possible energy conserved per phenazine molecule reduced. In biofilms, PCN is the phenazine produced and retained at the highest levels[33], making it of additional interest to our understanding of cell survival. In all experiments, a Δ*phz1/2* mutant was used that cannot synthesize phenazines, and PCN was exogenously provided at physiologically-relevant concentrations. Data analysis details and the rationale for using electrons sec^{-1} units, as opposed to Watts, when reporting metabolic rates are provided in the Supplemental Information.

PCN EET promotes anaerobic survival at extremely low metabolic rates

We first conducted weeklong PCN anaerobic survival assays as previously reported[22] to compare survival phenotypes on PCN to those previously made for other phenazines and make metabolic rate measurements. Cells were incubated anaerobically in large, well-mixed, custom glass electrochemical reactors connected to potentiostats poised to re-oxidize the PCN reduced by the cells (Figure 1C). Samples were removed periodically from the reactors to measure colony forming units (CFUs). After one week of incubation at 33˚C, cultures provided with PCN and a re-oxidizing potential (+PCN/pot) lost less than an order of magnitude of their initial viability while anaerobic cultures incubated in the same medium -PCN/pot lost viability by three orders of magnitude (Figure 1D). At the end of the incubation, we measured the cumulative acetate produced by the cells (as a consequence of the oxidative arm of the facilitated fermentation, pyruvate ⇒ acetate, Figure 1B), finding it to be 122±34 μmoles (n=2), approximately balanced

with the total PCN reduced (the reductive arm), 107±4 μmoles (n=2), as expected (See Supplemental Information for details). The amount of acetate produced was also an order of magnitude higher in the +PCN/pot than the -PCN/pot cultures (Figure 1E), in agreement with our working model (Figure 1B). To assess the percentage of cells that were metabolically active in these different conditions, we stained culture samples on day 5 with the fluorescent viability dye propidium iodide (PI is taken up when cells are metabolically and/or physically compromised), finding that the majority (88%, n=794 cells) of -PCN/pot cells fluoresced brightly whereas very few (2.4%, n=830 cells) +PCN/pot cells were fluorescent (Figure 1F). Notably, the population sustained by PCN cycling appeared to be homogeneous with respect to PI staining. Taken together, these results are consistent with PCN EET powering a facilitated fermentation that enables anaerobic survival, similar to what we have observed for other phenazines[22].

Recently, Hoehler et al.[34] collated a large dataset of metabolic rates measured across all life on Earth to estimate the average mass-specific basal metabolic rate of the biosphere. We wondered how the metabolic rate of PCN survival would compare to both bacterial measurements and other organismal measurements in their published dataset. We summarize our findings here, with a more detailed accounting of our analysis of our samples and the Hoehler et al. dataset found in the Supplemental Information. Consistently, the current produced by the +PCN/pot cultures during their survival is characterized by an initial spike, followed by a decrease in current to a steady state held between days one and seven (Figure 2A). Given the spike occurs before the onset of death in the -PCN/pot condition, this likely reflects adjustment of the cells to a new condition and thus we interpret the lower, stable current as the survival metabolism. Averaging this current and the associated CFUs across days one to five, we estimated the bulk cell-specific metabolic rate of the surviving cells to be 1.6×10^{3} electrons sec^{-1} $cell^{-1}$ at 25˚C (lower 95% CI 8.6×10^{2}, upper 3.1×10^{3}). To transform units of $cell^{-1}$ to $(g\ C)^{-1}$, we measured the average cell dry weight of +PCN/pot cells. Contrary to expectations for cell size when challenged by extreme energy limitation[7,35] the cells were not especially small; we measured their dry weight on day five to be $2.0\pm0.1 \times 10^{-13}$ g $cell^{-1}$, comparable to measurements of various species in the early stationary phase of growth[36]. Assuming a $\Delta G'^{\circ} = -65.6$ kJ $(mol\ PCN\ reduced)^{-1}$ (see Supplemental Information), our estimate of the cell-specific metabolic rate is equal to a mass-specific power of 8.7×10^{-4} W $(g\ C)^{-1}$ (lower 95% CI 4.7×10^{-4}, upper 1.7×10^{-3}). This value is about one order of magnitude below the average basal metabolic rate across all organisms reported by Hoehler et al., 1.2×10^{-2} W $(g\ C)^{-1}$. Under the conditions of our assay, the PCN EET mass-specific metabolic rate falls within the lower 2% of measurements across all organismal groups, and among those groups, only the gelatinous invertebrates are noticeably lower[34]. An alternative analysis that

includes the contribution of the initial current spike via an integration approach (across days 0 to 5) resulted in a slight increase in this estimate with an average cell-specific metabolic rate of 1.7 x 10^3 electrons sec^{-1} $cell^{-1}$ and a corresponding mass-specific power of 9.3 x 10^{-4} W $(g\ C)^{-1}$.

We then sought to further contextualize this metabolic rate across the hundreds of bacterial measurements in the dataset. To avoid the accumulation of potential errors stemming from assumptions about how much energy is conserved per electron transferred, we analyzed the cell-specific metabolic rates in units of electrons sec^{-1} $cell^{-1}$. Notably, across disparate catabolic pathways the ratio of ATP generated per electron transferred varies by less than an order of magnitude, a fact that to our knowledge has not been recognized. For example, the PCN survival metabolism using glucose has an energy conservation ratio of 0.5 ATP $electron^{-1}$ while aerobic catabolism of glucose is 1.3 ATP $electron^{-1}$ (Supplemental Information). Given these values represent disparate metabolisms yet do not deviate far from unity, we conclude that within this dataset that is dominated by measurements of glucose metabolism and aerobic respiration rates, units of electrons have an approximate equivalency to ATP units of energy, and therefore transformed the values originally reported in the primary publications collected by Hoehler et al. to units of electrons sec^{-1} $cell^{-1}$ (see Supplemental Data Table for full dataset).

Within the categories of bacterial measurements, those reporting on endogenous metabolism, or the oxidation of endogenous carbon sources, contained the lowest and most heterogeneous values; the PCN EET cell-specific metabolic rate was in the lower 15% of them (Figure 2B). The maximum cell-specific metabolic rate of *P. aeruginosa* growing aerobically on glucose has been measured to be approximately 10^6 electrons sec^{-1} $cell^{-1}$ [37,38], three orders of magnitude higher than PCN EET, revealing that this organism has a remarkably plastic metabolic pace. We also found that the cell-specific metabolic rate of PCN EET, while supporting the maintenance of the population (Figure 1D), was nonetheless 2-3 orders of magnitude lower than maintenance metabolic rates inferred from continuous culture studies. This finding supports those of prior studies showing the metabolic rates of microbes in oligotrophic natural environments are significantly lower than the maintenance requirements predicted from continuous culture[5]. We conclude that PCN facilitated fermentation occurs at an extremely low cell-specific metabolic rate, a facet of this metabolism that was unappreciated previously.

PCN facilitated fermentation powers a non-growth maintenance state

Because PCN metabolism is positioned at the lower end of measured metabolic rates documented for any organism, we wondered whether the weeklong population survival phenotype

promoted by PCN EET reflected a non-growing survival state or a dynamic balance of growth and death, akin to the growth advantage in stationary phase phenomenon observed in *E. coli* under nutrient limitation[39]. To distinguish between these possibilities, we performed a pulse-chase experiment using the fluorescent cell wall stain 7-hydroxycoumarincarbonylamino-D-alanine (HADA), a stain that has been previously used in *P. aeruginosa* to monitor cell growth[40]. During bacterial growth, HADA is covalently incorporated into the cell wall, and after unincorporated HADA is washed away, new growth can be visualized as a loss of fluorescence in the non-pole regions of the cell[41] (Figure 3A). As a positive control, we checked to see whether we could observe HADA loss during anaerobic growth on nitrate[42]. As expected, HADA fluorescence was lost in a topological manner consistent with non-pole incorporation of new, non-fluorescent cell wall material (Figure S1) and was mostly diminished save for a few dimly fluorescent poles by day four (Figure 3B). HADA distribution over the cell body was unchanged after four days in the absence of nitrate (Figure 3B, S1). The presence of HADA in the cell wall did not affect the growth rate of the culture (Figure 3C).

Having validated HADA for *P. aeruginosa* in our medium, we applied it to observe cells in our electrochemical reactors. HADA-stained cells in the +PCN/pot condition retained HADA throughout the entirety of their cell wall over the course of seven days (Figure 3D, S1). Notably, some cells that had not finished dividing during the inoculum transfer from oxic to anoxic conditions had HADA-labeled septa that remained intact even after the seven days of anaerobic incubation (Figure 3D, inset). The presence of HADA did not affect the survival or viability loss of the +PCN/pot and -PCN/pot cultures, respectively (Figure 3E). Lastly, the HADA-labeled and unlabeled poles of at least 400 cells from each day and condition were counted to estimate the number of divisions across the population (Figure 3A). These values for each day were close to zero (Figure 3F). Our results indicate that cells are statically surviving without growth during anaerobic PCN EET, and we therefore conclude that facilitated fermentation, under these conditions, powers a non-growth maintenance state, a fact that hitherto was ambiguous.

While imaging cells from the -PCN/pot condition, we noticed in phase contrast that a significant number of cells displayed dark foci in their cytoplasm (Figure 3D), reminiscent of protein aggregates associated with ATP depletion and the viable but non-culturable (VBNC) state[43]. To test if this state explained the loss of cell viability in the -PCN/pot condition, throughout the anaerobic experimental time course, we subsequently incubated a sample of -PCN/pot cells in aerobic resuscitation conditions for two days before plating (see methods). At day seven of the anaerobic incubation, the CFU counts from the resuscitated cells were about two orders of magnitude higher than the counts from cells that were immediately plated (Figure S2B). The

remaining order of magnitude discrepancy between the +PCN/pot and -PCN/pot conditions, representing most of the population, was not recovered (Figure S2A). Consistent with this finding, cell pellets of the cultures on day seven showed a clear size disparity between the +PCN/pot and -PCN/pot condition, indicating significant amounts of cell lysis had occurred in this sample during anaerobic incubation (Figure S2C). We also confirmed that cells in the -PCN/pot condition were ATP-depleted relative to the +PCN/pot condition (Figure S2D), consistent with the presence of cells in the VBNC state[43]. We conclude that the majority of CFU loss in the -PCN/pot condition is caused by death, with a minor subpopulation entering a VBNC state.

A high throughput platform can advance our understanding of non-growth metabolism

While the preceding large reactor experiments enabled us to determine the pace of PCN EET metabolism relative to life's average basal metabolic rate and confirm it relies on a facilitated fermentation that fuels a non-growth metabolism, large reactors are cumbersome and low-throughput, limiting our ability to explore diverse conditions and mutant strains—variables that are essential to study when seeking a mechanistic understanding of a biological phenomenon. Recently, a 96-well electrochemical system was developed[30]. This system employs printed carbon electrodes on the bottom of each well, allowing for independent, multiplexed potentiostatic measurements (Figure 4A). To determine whether we could conduct PCN anaerobic survival assays in similar ways between the large and high throughput reactors, we compared survival phenotypes quantitatively. Under the same conditions (i.e. medium and PCN concentration) in the high throughput platform, cells survived several orders of magnitude better in the presence of PCN and an oxidizing potential, as observed for the large reactors, yet we were additionally able to test many other concentrations of PCN because of the increased throughput (Figure 4B). While the primary trends were conserved between the reactors, cells died at an even faster rate in the absence of PCN in the high throughput system, and all cultures, regardless of the PCN concentration, lost viability after day 5. Accordingly, we terminated experiments in the high-throughput reactor platform at day 5. While the amount of survival measured in this system at 75 μM PCN was about half of that measured in the large reactor system by the end of the experiments, it was still less than an order of magnitude total loss in survival (Figure 4B, table).

Encouraged by these findings, we leveraged the high throughput platform to gauge the antibiotic tolerance of cells in the non-growth state supported by anaerobic PCN-cycling. After a day of incubation in the 96-well device, we added five different drugs representing distinct antibiotics that target different cellular processes: ceftazidime, a β-lactam that targets cell wall

synthesis; ciprofloxacin, a fluoroquinolone that disrupts DNA gyrase; tobramycin, an aminoglycoside that interferes with protein synthesis; N,N-dicyclohexylcarbodiimide (DCCD), an F_OF_1 ATP(synth)ase inhibitor; and colistin, a polymyxin that disrupts the cell membrane. Cell viability was mildly impaired by ceftazidime and ciprofloxacin, moderately by tobramycin, and greatly impacted by DCCD and colistin (Figure 4C). These results resemble tolerance profiles that have been observed for cells in the non-growing anoxic cores of *P. aeruginosa* biofilms that are metabolically sustained by phenazine EET[11,20,44], pointing to the importance of maintaining membrane integrity[45,46] and bioenergetic activity to preserve viability in the absence of growth.

Cells are energy-limited and surviving near their maintenance requirement

Having validated the utility of our high throughput PCN-cycling assay to study a clinically-important cellular state, we proceeded to measure the survival of hundreds of cultures across various mutant strains over a range of PCN concentrations with multiple tiers of replication to begin to mechanistically dissect it (Figure 5A). First, we sought to define the facilitated fermentation metabolic pathway more precisely by comparing mutant strains lacking enzymes of bioenergetic importance that we hypothesized might contribute to PCN-based survival[24,47]. Second, we sought to determine whether the amount of PCN cycling was limiting survival. We achieved these goals by leveraging knowledge that the amount of current generated via EET is proportional to the concentration of electron shuttle provided[48]. Hypothesizing that the PCN concentration would therefore limit the total culture's metabolic rate, we made measurements across PCN concentrations spanning three orders of magnitude (Figure 5A).

After five days of anaerobic incubation in our high-throughput platform, we found that survival of the Δ*phz1/2* strain was dose-dependent up to at least 75 μM, with increasing concentrations having only marginal effects on survival (Figure 5B). Phenazine reduction can occur promiscuously via multiple metabolic flavoproteins[49,50], but we have shown recently that PCN is predominantly reduced in stationary phase cells by two NADH dehydrogenases in the cell membrane, Nuo and Nqr[47] (Figure 1B). While the current produced by a Δ*phz1/2* Δ*nuoF* Δ*nqrF* mutant was initially lower, after a day it approximately equaled that of the Δ*phz1/2* cells, suggesting other PCN reductases compensate after this time (Figure 5C). However, full survival across PCN concentrations nonetheless depended upon functional NADH dehydrogenases (Figure 5B) with the loss of viability in their absence occurring steadily over the entire course of the incubation (Figure S3A), consistent with our working model (Figure 1B). Complementation of either NADH dehydrogenase restored survival at most concentrations of PCN, indicating they

serve largely redundant functions (Figure S3B). As a negative control, and in agreement with our previous study[24], knocking out the AckA-Pta pathway (the energy-conserving step of the metabolism) had a larger consequence upon survival. Moreover, our platform allowed us to measure survival of this mutant across many PCN concentrations efficiently, something that would have been logistically impossible using large reactors. Interestingly, increasing PCN concentrations resulted in increased survival of the Δ*phz1/2* Δ*ackA-pta* mutant, albeit at significantly lower levels (Figure 5B). We hypothesized that this alternative mode of phenazine-dependent survival might also rely on the NADH dehydrogenases, and therefore tested a Δ*phz1/2* Δ*nuoF* Δ*nqrF* Δ*ackA-pta* mutant. Though this strain's survival was lower than the Δ*phz1/2* Δ*ackA-pta* mutant, it still improved up to 75 μM PCN, yet did not improve in survival at higher concentrations of PCN, indicating that the NADH dehydrogenase complexes play a significant role at these concentrations (Figure 5B). Overall, our data are consistent with substrate-level phosphorylation being the primary energy conserving mechanism under these conditions (Figure 1B) but also indicate the existence of a previously undetected, alternative PCN-dependent energy conservation pathway that supports much lower levels of survival.

We also measured the long-term current generated by Δ*phz1/2* as a function of PCN concentration and found the two were largely correlated, as expected[48] (Figure 5D). As with the large reactors, we observed an early spike in current generation dependent on the phenazine concentration provided that then subsided to a lower, more stable current, though the decay happened at a slower rate than in the large reactors (Figure 5C, Figure 2A). The one exception was at 750 μM PCN, which produced highly variable initial currents despite stable currents later (Figure 5C). By integrating the current generated between days one and five (i.e. after the initial current spike), we calculated the average PCN oxidation rate across PCN concentrations and found it unexpectedly saturated above 75 μM (Figure 5D). At 375 μM PCN, the current measured on days 1-5 was below what the electrode was capable of oxidizing, exemplified by the initial high current spike (Figure 5C). What might cause this later saturation? We hypothesized that either PCN oxidation at the electrode was limiting due to biofouling, or the rate of PCN reduction was limiting due to a change in the cells that occurs after a day of anaerobic incubation.

To distinguish between these scenarios, we used scanning electron microscopy to visualize cells on the electrodes, finding that the electrodes were mostly clear with a sparse monolayer of cells present on the working electrode surface, with the densest cell monolayer found in the 375 μM PCN condition (Figure S4A). While the absence of biofilms on the electrode suggested that biofouling was unlikely to explain the observed reduction rate plateau, we sought a more direct test of whether the cells or the electrode was limiting. Accordingly, on day 5 of the

survival assay, we pooled Δ*phz1/2* cells from multiple technical replicate wells in the 375 μM PCN condition, pelleted them, resuspended them in a small volume and added them to other wells containing Δ*phz1/2* cells and 375 μM PCN such that the total cell concentration was approximately doubled. We observed a 1.5x increase in current generation following the increase in cells that was sustained for at least 10 hours (Figure S4B), demonstrating that the electrode was not limiting. Accordingly, the observed PCN oxidation rate at the electrode (Figure 5D) can be interpreted as equivalent to the cellular PCN reduction rate. Our results suggest that after about one day in anaerobic conditions, the cellular reduction rate above a certain PCN concentration becomes attenuated. This finding is intriguing, as bacteria are believed to always maximize their metabolic rate to maximize fitness during growth[51,52]. What explains this attenuation is a worthy subject for future studies, especially given that these PCN concentrations are in the range found in *P. aeruginosa* biofilms[33].

Finally, we sought to determine whether the power output of the PCN facilitated fermentation was at or above the minimum necessary for maintenance metabolism under PCN-cycling conditions. We reasoned that we would observe a relatively constant cell-specific metabolic rate over the PCN concentration range if this were true, as that would indicate that surviving cells require the same metabolic rate. Indeed, this is what we observed (Figure 5E). The cell-specific metabolic rate measured at 75 μM PCN was 3.0×10^3 electrons sec^{-1} $cell^{-1}$ at 25˚C (lower 95% CI 1.6×10^3, upper 5.4×10^3), slightly higher than the rate measured in the large electrochemical reactors. Given the PCN concentration limits survival between 0.75 and 75 μM (Figure 5B), this consistent metabolic rate suggests that PCN limitation imposes an energy limitation, reducing the populations' viability in a PCN-dependent manner. While a fraction of cells may be in the VBNC state that are not accounted for in this analysis, particularly at lower PCN concentrations, such cells would be expected to make a minor contribution to the overall current measured[6]. We therefore conclude that the culturable cells are operating near their minimum maintenance power requirement for these conditions.

DISCUSSION

That bacteria can survive for remarkably long periods of time when limited for nutrients or energy is well known, yet the question of how cells maintain viability in the absence of growth has been challenging to answer due to technical limitations. Answering this question is important for both fundamental and practical reasons: growth arrest not only typifies bacterial existence in most natural habitats, but also in disease contexts. Indeed, our inability to successfully treat chronic

infections wherein cells are metabolically active yet doubling very slowly or not at all, stems in large part from our ignorance of the molecular strategies that sustain life during growth arrest. Our work here demonstrates that it is possible to gain mechanistic insight into the maintenance physiology of *P. aeruginosa* by investigating how it cycles the phenazine PCN under anoxic conditions—a non-growth state operating at an extremely low power output that lends itself to quantitative studies in high throughput.

When surviving anaerobically via PCN cycling, *P. aeruginosa* cellular integrity and metabolic activity is sustained at the cell-specific metabolic rate of 1.6 x 10^3 electrons sec^{-1} $cell^{-1}$ at 25 ˚C, equivalent to a mass-specific metabolic rate of 1.6 x 10^{16} electrons sec^{-1} $(g\ C)^{-1}$ or roughly 10^3 ATP sec^{-1} $cell^{-1}$. The term basal power requirement has been introduced to define the minimum bioenergetic power per unit biomass required to sustain metabolic activity[5]. In our system, cell survival is limited by a required minimum cell-specific metabolic rate (Figure 5E) suggesting this rate may represent the basal power requirement for *P. aeruginosa* under these conditions. Remarkably, this rate lies 3 to 4 orders of magnitude below the energy demand during fast aerobic growth (Figure 2B), highlighting the extraordinary range of power output that a single bacterial species can use to support its metabolism and helping to explain its success as an agent of both acute and chronic infection. Recently, multiple environmental measurements of microbial cell-specific metabolic rates under energy-limitation have also been made or modeled[53], adding to a short list of basal power requirement estimates. Measurements of oxygen consumption below the seafloor of the North Pacific Gyre were found to reach an asymptote at depth around 25 electrons sec^{-1} $cell^{-1}$, with the temperature unreported but presumably cold[54]. The cell-specific metabolic rate of anaerobic sulfate-reducing bacteria found below the seafloor at multiple sites were measured to reach an asymptote at depth to about 2.8 x 10^2 electrons sec^{-1} $cell^{-1}$ at temperatures around 5˚C[55]. Bacteria residing beneath permafrost in the cryopeg brines of Utqiaġvik, Alaska have been modeled to sustain metabolic rates between 18 and 1.7 x 10^3 electrons sec^{-1} $cell^{-1}$ at subzero temperatures[56]. When these measurements are adjusted to 25˚C assuming a typical Q_{10} normalization[57], they fall surprisingly close in order of magnitude to our measurements in the lab (Figure 2B). Given the uncertainties underpinning assumptions needed to assign metabolic rates to environmental datasets, it is conceivable that our lab measurement and true environmental basal power requirements converge upon the fundamental limit of what is needed to power bacterial survival, or otherwise, converge to the limit of what is measurable with current methods. More quantitative studies of diverse maintenance states will be needed to determine whether such a conserved minimum exists.

It is generally believed that organisms in the environment metabolizing at low rates are growing, albeit slowly; indeed, environmental doubling times on the order of days to 1000s of years have been estimated by multiple studies[58]. Accordingly, anticipating that PCN cycling would power slow growth, we were somewhat surprised that cell growth was not detectable using our HADA assay (Figure 3D). It may be that we simply did not wait enough time to observe slow growth in the lab and/or that estimates of slow growth in the environment are inexact. To parse this discrepancy, we note that it has been estimated that the energetic cost of aerobic division for a bacterial cell is approximately 4×10^9 ATP per division[59]. Based on the dominant ATP-generating pathway used under these conditions (i.e. oxidation of glucose to acetate coupled to substrate-level phosphorylation, Figure 1B), we estimate that *P. aeruginosa's* ATP output is about 8.0×10^2 ATP sec^{-1} $cell^{-1}$. We can then estimate that if division were possible under PCN facilitated fermentation, cells would be doubling at a rate of once every two months, and perhaps even faster because biosynthetic costs are thought to be less under anoxic conditions[60] and the fraction of energy lost to maintenance processes is presumed to be less during slow growth[61]. Such a growth rate should have been detectable with our assay, corresponding to a steady increase to at least ~0.125 divisions in a week, yet instead we observed division values consistently centered around 0 (Fig 3F). Thus, it seems more likely this ATP output is the maintenance energy requirement. Together, this reasoning prompts us to question whether microbes are capable of doubling on exceedingly-long time scales, or if they instead undergo long-term survival, opportunistically waiting for punctuated bursts of local nutrients to fuel relatively fast growth as has been suggested recently[62]. In this way, the classic "feast-famine cycle" may apply to more than just enteric bacteria[63], which would carry implications for biogeochemical modeling[64]. Future studies of the growth associated with extremely slow metabolic rates are needed to determine which model is more accurate.

Leaving such speculation aside, a consequential feature of PCN cycling fueling a non-growth state is that it opens the door to the identification of cellular strategies that sustain maintenance more broadly. In our system, EET provides a convenient way to quantify metabolic rate and stabilize a non-growth state, yet some of the physiological strategies underpinning maintenance during PCN-cycling are likely to overlap with those required during non-EET survival[65]. Given that non-growing cells tolerate conventional antibiotics but are sensitive to drugs that target membrane and bioenergetic components (Figure 4C), we elucidated the key catabolic enzymes supporting survival during PCN cycling as a proof-of-concept that our high throughput platform can be used to gain mechanistic insight into what underpins a low-power lifestyle. By focusing on PCN's role as an electron acceptor, we expected to identify machinery that specifically

interacts with PCN, yet we anticipate that future studies of the maintenance state supported by PCN will identify more general physiological strategies that sustain a low-power energy economy.

While we previously established that the AckA-Pta enzymes are necessary for phenazine facilitated fermentation[24], our work here revealed that either of the NADH dehydrogenases Nuo and Nqr are additionally necessary to support full survival of cells via PCN facilitated fermentation (Figure 5B). This may only apply to the phenazine PCN, as we have shown that it is the only derivative made by *P. aeruginosa* that is predominantly reduced at the inner membrane[47]. Indeed, phenazines are known to promiscuously react with many metabolic flavoproteins in the cytosol[49,50]. This promiscuity likely explains our finding that increasing concentrations of PCN correlated with increasing survival in the Δ*phz1/2* Δ*nuoF* Δ*nqrF* mutant tested (Figure 5B). We speculate that the benefit the NADH dehydrogenases provide is a direct coupling to the NADH pool and, by extension, pyruvate oxidation. While other flavoproteins can dissipate reducing equivalents onto the PCN pool in the absence of the NADH dehydrogenases, the reductants involved may not be as closely coupled to the NADH pool and be wasted energetically. The PCN-dependent compensation of the Δ*phz1/2* Δ*ackA-pta* mutant (Figure 5B) is more difficult to explain and suggests the participation of unidentified alternative energy-conserving pathways. These pathways may still be NADH-coupled, which could explain the loss of enhanced survival in the Δ*phz1/2* Δ*ackA-pta* mutant at high PCN concentrations in the Δ*phz1/2* Δ*nuoF* Δ*nqrF* Δ*ackA-pta* mutant (Figure 5B). Future metabolomic experiments will shed light on the nature of these PCN-dependent compensations.

In their normal function during respiratory growth, the Nuo and Nqr complexes chemiosmotically pump protons across the cytosolic membrane with $H^+/2e^-$ of 4 and 2, respectively[66,67]. This is driven by a large $\Delta E^{\circ\prime}$ of 420 mV between the NADH and ubiquinone pools. For PCN reduction by NADH, $\Delta E^{\circ\prime}$ is less than half that value at 180 mV, corresponding to a $\Delta G^{\circ\prime}$ of −34.7 kJ/mol. Previous work has estimated the minimum biological energy quantum (enough to drive the translocation of one proton across the cytoplasmic membrane) to be −20 kJ/mol[68]. These values may change some amount depending on the reaction context, namely concentrations of reactants and products and the PMF level, but provide a useful quantitative baseline. From these values, we infer that PCN reduction by an NADH dehydrogenase theoretically provides only enough free energy to translocate one proton, less than the normal proton coupling of Nuo and Nqr. Additionally, phenazines have been shown to be reduced via flavin active sites of other metabolic redox enzymes[49], and if this also applies to the NADH dehydrogenases (i.e. reduction at the NADH binding site), it seems unlikely that PCN reduction would trigger the enzymatic conformational changes necessary to pump protons. However, if

phenazines were reduced at the ubiquinone binding site (permitting the proper conformational changes for proton pumping) and the cell were under low PMF conditions, proton pumping might be possible, as metabolic reactions operating near their thermodynamic equilibrium are known to occur[69]. Further studies using purified Nuo and Nqr with phenazine substrate are needed to determine if this mechanism of energy conservation is plausible.

Outside of its fundamental interest to cell biology, understanding the minimal energy requirements and physiology of cells in a non- or slow-growth state has important practical implications. Despite the fact that estimated microbial doubling times in nature typically are on the order of days to weeks to years[70–73], the vast majority of microbial physiology studies in pure culture have been conducted using model species grown with doubling times under an hour. The consequences of this nature-to-lab metabolic rate mismatch has resulted in our inability to control non- and slow-growing microbes in nature and disease. In addition to the deleterious impact this knowledge gap has for biofilm control in chronic infections as we have discussed, if synthetic biologists are to succeed in catalyzing desirable changes in the field, such as applying pro-biotics to the rhizosphere to stimulate the growth of crops, they will require a deeper understanding of how cells survive periods of growth arrest due to desiccation or nutrient limitation[74,75]. Moreover, identifying the slowest viable metabolic rates and what permits them would help geobiologists and climate scientists better understand the fate of organic matter soils and sediments, where the crucial roles of microbes are widely recognized but challenging to model[64,76,77]. In all these cases, an understanding of life “in the slow lane”, is needed[62]. Our PCN-cycling system opens the door to quantitative and mechanistic studies of a maintenance state that comes much closer to approximating real-world non-growth metabolisms than the typical growth conditions used in the lab.

Finally, while bioenergetic comparisons often rely on thermodynamic arguments to compare the energy conservation efficiency of different metabolisms, our results highlight the importance of kinetics in explaining the remarkable plasticity of microbial metabolism. To wit: per glucose molecule, fermentation generates roughly 10 times less ATP than aerobic respiration, yet the cell-specific metabolic rate during facilitated fermentation we measure is 1,000 times slower than *P. aeruginosa*’s fast aerobic growth. In terms of power, this disparity is dominated not by differences in energy conservation efficiency but by differences in rates. Indeed, it seems likely that slow kinetics may dominate the bioenergetic reality of low-power maintenance metabolism, as previously suggested[7]. If, how, and when metabolic rate is controlled by the cell at the molecular level or limited by the environmental conditions imposed are important questions to be

addressed in future research and key to an understanding of the dominant pace of microbial life on the planet.

Limitations of the Study

In this study, we have leveraged an EET metabolism to develop a quantitative, high-throughput system for studying a low-power maintenance state. While the mechanistic studies we described focused on identifying catabolic machinery necessary for survival via PCN EET (e.g. NADH dehydrogenases), parts of these pathways are needed to sustain survival in other contexts (e.g. the AckA pathway is also necessary for survival when oxygen is limiting in the absence of EET[65]). Future studies will reveal which other pathways (e.g. anabolic, regulatory) sustain the needs of cells in the PCN-maintenance state and whether they are more broadly conserved across bacteria existing in a non-growth state, be they other opportunistic human pathogens or bacteria in arid soils or deep-sea sediments. While it is likely that some cellular maintenance strategies will be specific for particular organisms in specific contexts, we expect others may be more generalizable.

The system used to assess this metabolism, both in large reactors and the 96-well platform, is an artificial planktonic reconstitution of a metabolism that is more naturally relevant to biofilms[33,78]. Thus, it is important to acknowledge there may be differences in the metabolic dependencies of cells in this planktonic state versus the more natural biofilm state. However, many key features that characterize biofilm cells are recapitulated in this system, including a lack of growth in the anoxic core and lowered metabolic activity[79], features that contribute to antibiotic tolerance[11].

Finally, we note that the anaerobic survival assessed in this study is not a state of perpetual survival: cells begin to die after 7-9 days in the large reactors and after 5 days in the 96-well plate system. Therefore, the cells have been assessed in the middle of a quasi-steady-state that may or may not be representative of cells under a maintenance state in nature or disease, though they are probably much more representative than cells cultivated in chemostats that achieved stable but slow, constant growth. Cells were assessed in only one medium during this study, so variations in metabolic rate and active metabolic pathways as a function of physiological conditions were unexplored. Bacteria do not have a defined basal metabolic rate, so our finding that phenazine EET is an order of magnitude slower than the basal metabolic rate of the biosphere is an imperfect comparison—one that we view as informative for understanding the relative positioning of phenazine facilitated fermentation among all metabolic rates. While the

rate is slow, as we note in the results, it falls in the ~15th percentile of endogenous metabolic rates previously measured in bacteria. Therefore, it is not the slowest metabolic rate measured, but to our knowledge it is currently the only one proven to be coupled to a non-growth maintenance state at the single-cell level.

ACKNOWLEDGEMENTS. This work was supported by NIH Grant (2R01AI127850-06A1) to DKN. This work was supported by JSPS KAKENHI (22H02265 and 22KK0242), and JST GteX (JPMJGX23B4) to AO. We are grateful to Georgia Squyres and Sean Wilson for their help with the HADA experiment, and Avi Flamholz and other members of the Newman lab for constructive feedback throughout the study.

AUTHOR CONTRIBUTIONS

Conceptualization, J.A.C., A.O., and D.K.N.; Methodology, J.A.C., C-L.H., R.D.H., A.O., and D.K.N.; Investigation and Validation, J.A.C., C-L.H., and R.D.H.; Formal Analysis and Visualization, J.A.C.; Resources, A.O. and D.K.N. Writing – Original Draft, J.A.C. and D.K.N.; Writing – Review & Editing, J.A.C., C-L.H., R.D.H., A.O., and D.K.N.; Supervision and Funding Acquisition, A.O. and D.K.N.

DECLARATION OF INTERESTS

The authors declare no competing interests.

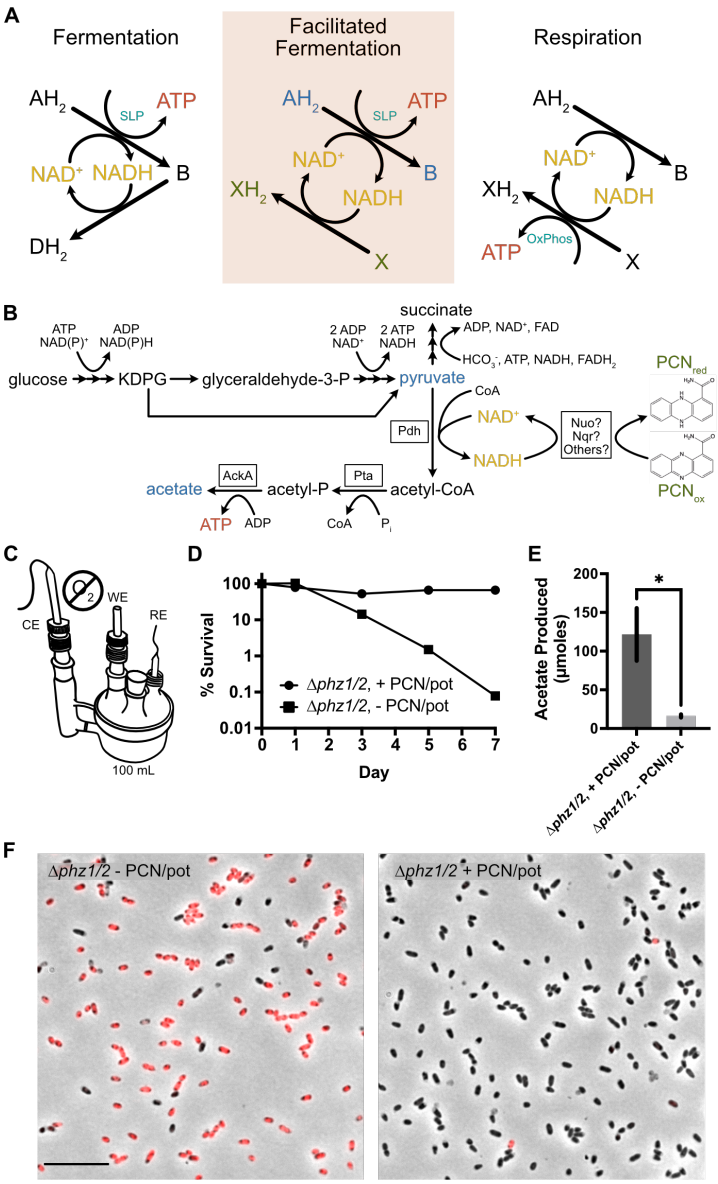

1

Figure 1. PCN redox-cycling promotes anaerobic energy conservation and survival via a facilitated fermentation. (A) Simplified schema of heterotrophic metabolisms and their predominant mode of energy conservation, exemplifying how facilitated fermentation is a noncanonical form of energy conservation. SLP – substrate level phosphorylation, OxPhos – oxidative phosphorylation. (B) Working model of the active metabolic pathways catabolizing glucose during PCN facilitated fermentation. The NADH dehydrogenases Nuo and Nqr are putatively involved in the metabolism because of their previously established function as key PCN reductases[47]. (C) Schematic of large glass electrochemical reactors used in this study to continuously re-oxidize PCN anaerobically reduced by the cell culture. A stir bar in the main chamber kept the culture well-mixed. CE – counter electrode, WE – working electrode, RE – reference electrode. (D) Anaerobic survival of Δ*phz1/2* strain in glucose minimal medium with or without 75 μM PCN and an oxidizing potential. 100% survival represents approximately 8 x 10^8 CFU mL^{-1}. Data are representative of 4 biological replicates. (E) Quantification of acetate production after 7 days of culture incubation. Data are averaged across 2 biological replicates, error bars represent the standard deviation. Welch's t-test was used to compare samples, *p<0.05. (F) Propidium iodide staining of anaerobic cultures on day 5 of survival imaged on a fluorescence microscope. Images are representative of 2 biological replicates. Scale bar is 10 μm.

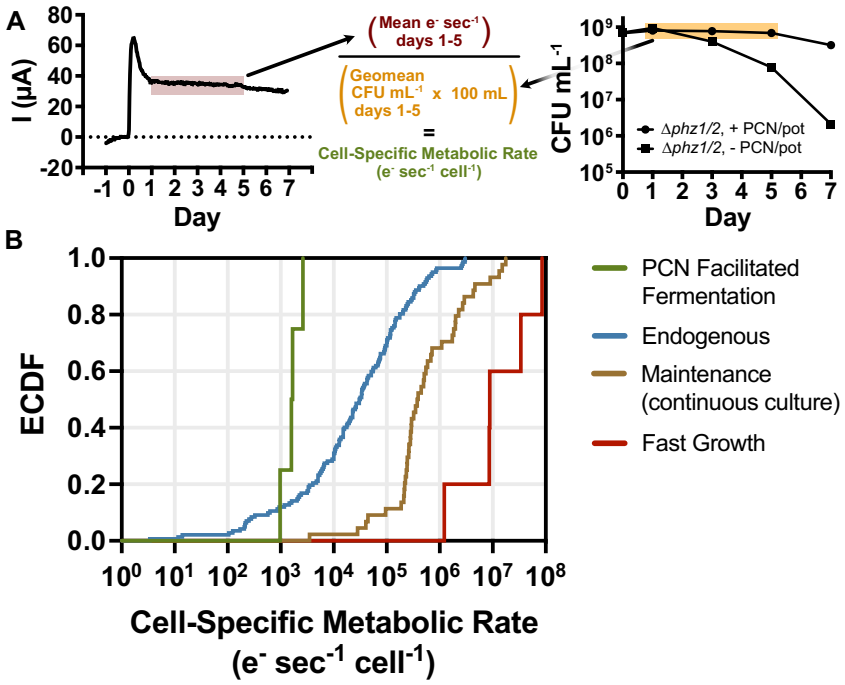

Figure 2. The metabolic rate of PCN facilitated fermentation is extremely low. (A) Cell-specific metabolic rate during PCN facilitated fermentation was quantified from large electrochemical reactor experiments. Cells are added on day 0. The mean current generated by the culture across days 1 to 5 was averaged and divided by the geometric mean of total CFUs across the same period. Data are representative of 4 biological replicates. (B) Empirical cumulative distribution functions of lab-measured bacterial metabolic rates collated previously by Hoehler et al.[27], with units transformed to electrons sec^{-1} $cell^{-1}$ at 25˚C. Fast growth includes bacteria growing at or near their maximum growth rate. Maintenance includes inferred maintenance energy metabolic rates (i.e. during zero growth) extrapolated from slow-growing continuous culture studies. Endogenous includes metabolic rates measured in the absence of any exogenous electron donor and using endogenous stores of donors instead. Each data point is an independent experimental measurement. The dataset encompasses 90 species and 198 measurements.

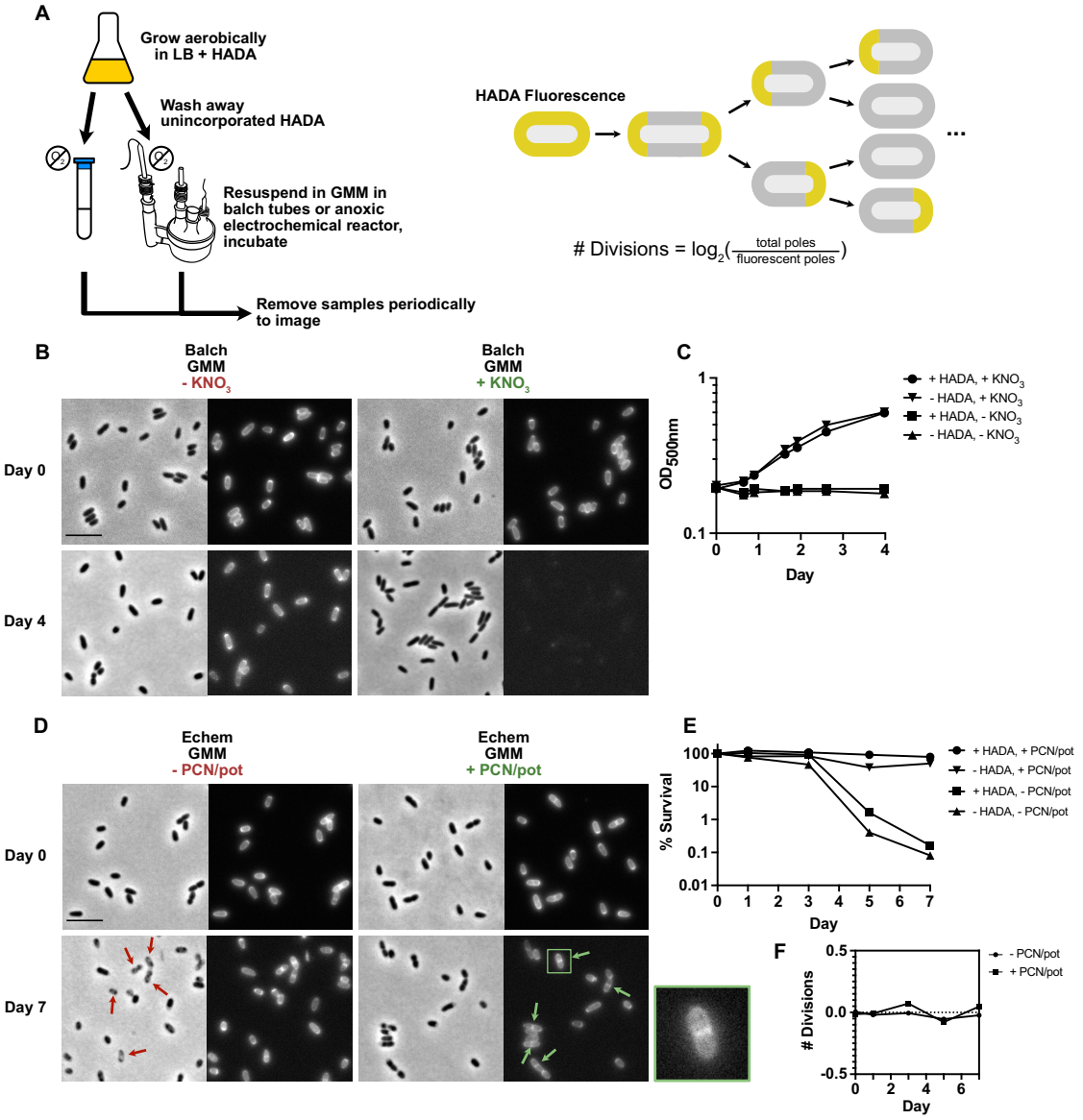

Figure 3. Single cells do not grow during anaerobic survival via PCN facilitated fermentation. (A) Experimental design and expected topological dilution of HADA cell wall stain during cell division. (B) HADA fluorescence imaging of cells during anaerobic growth on glucose and nitrate in sparged balch tubes. GMM – glucose minimal media. Scale bar is 5 μm. (C) Anaerobic growth of cultures imaged in (B) compared to cultures that were not stained with HADA. (D) HADA fluorescence imaging of cells during anaerobic survival on glucose, PCN, and an oxidizing potential in large electrochemical reactors. Scale bar is 5 μm. Red arrows indicate phase-dark granules that accumulate in cells that are not provided with PCN and an oxidizing potential. Green arrows indicate HADA-labeled septa that remained intact over the week-long incubation - inset is a zoomed example, each edge is 3.75 μm. (E) Anaerobic survival of cultures imaged in (D) compared to cultures that were not stained with HADA. (F) Estimated number of divisions of the +PCN/pot culture imaged in (D) via manual counting of fluorescent vs total cell poles and use of the equation in (A). Each datapoint is n≥400 cells. All data in figure are representative of two biological replicates.

1

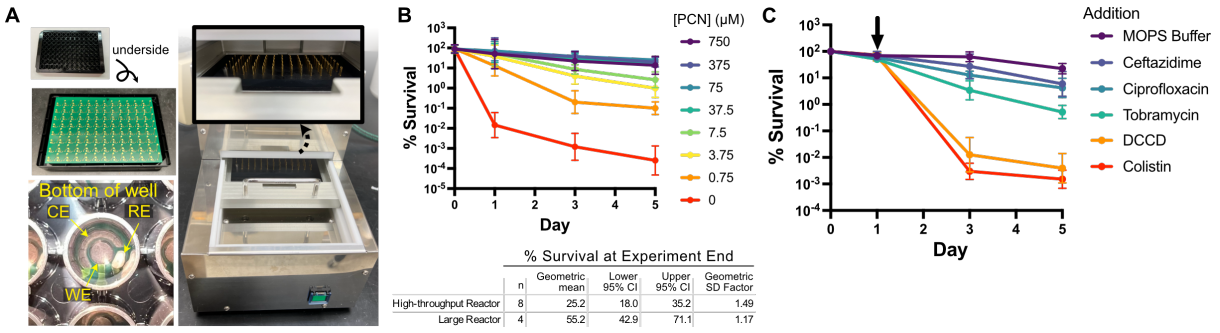

Figure 4. High-throughput electrochemical reactor system allows for multiplexed phenazine-dependent anaerobic survival assays. (A) 96-potentiostat plate reader used for experiments. Each well of the plate is outfitted with an independent working electrode (WE), counter electrode (CE), and reference electrode (RE) that are connected to the pins of the potentiostats via contacts on the bottom of the plate. (B) Anaerobic survival of Δ*phz1/2* strain in glucose minimal medium at various concentrations of PCN, with an oxidizing potential. Table – quantitative comparison of survival at experimental end (5 days in high-throughput reactor, 7 days in the large reactor), where n represents the number of biological replicates. (C) Anaerobic survival of Δ*phz1/2* strain in glucose minimal medium with 75 μM PCN and an oxidizing potential after various antibiotics were added on Day 1. Ceftazidime – 100 μg/mL, Ciprofloxacin – 10 μg/mL, Tobramycin – 100 μg/mL, DCCD – 2 mM, Colistin – 10 μg/mL. In both (B) and (C), 100% survival represents approximately 8 x 10^8 CFU mL^{-1}. Each datapoint represents the geometric mean of 8 biological replicates and error bars represent the 95% confidence interval.

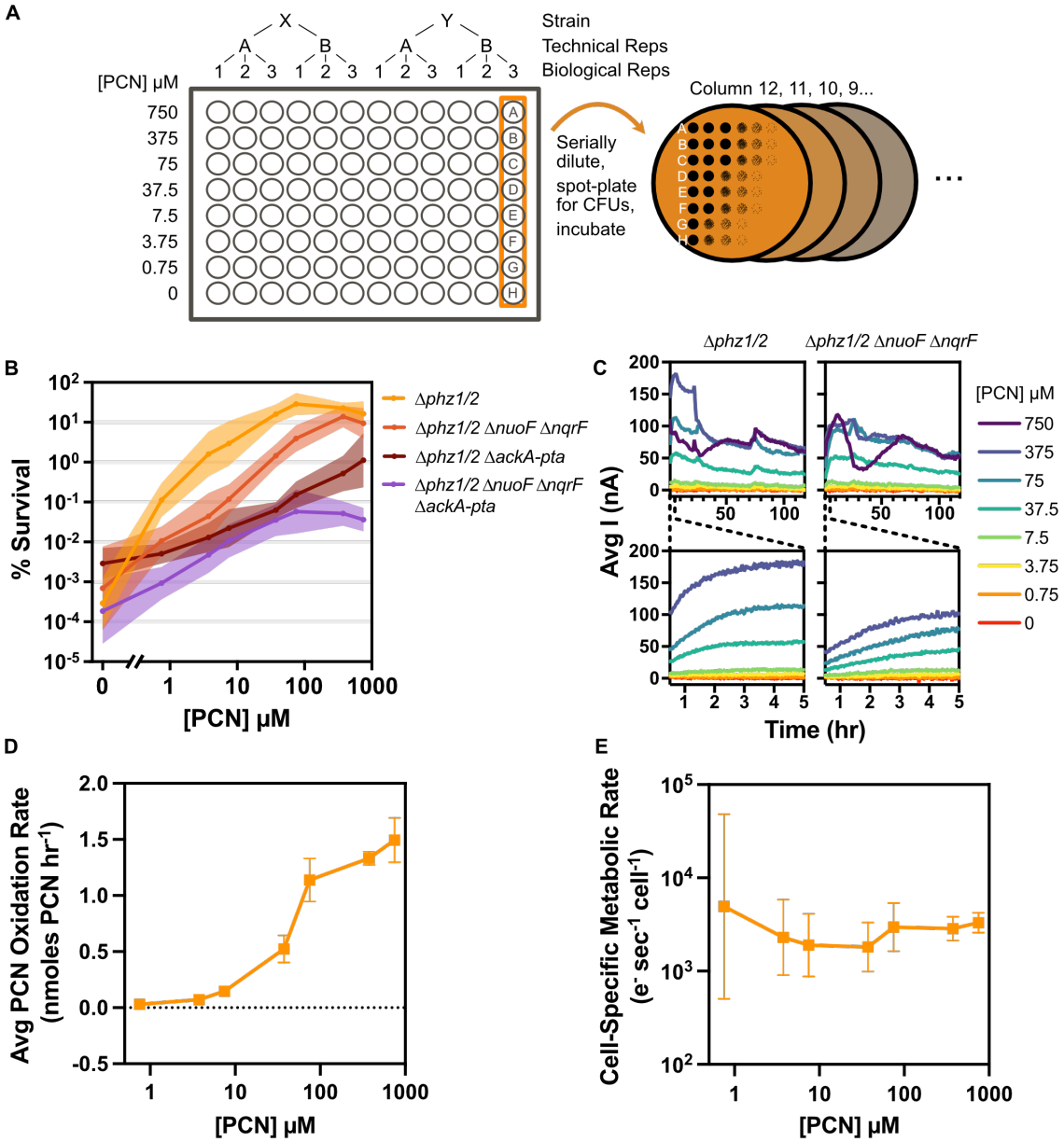

Figure 5. High-throughput PCN redox-cycling experiments reveal a dependence on NADH dehydrogenases and survival near the minimum maintenance requirement. (A) Example experimental design of high-throughput PCN redox-cycling survival experiments. (B) Survival of Δ*phz1/2* and metabolic mutant strains after 5 days of anaerobic incubation in a glucose minimal medium across various concentrations of PCN. Each datapoint is the geometric mean of at least 5 biological replicates. Shaded regions represent 95% confidence intervals. 100% survival represents approximately 8 x 10^8 CFU mL^{-1}. (C) Average current produced by Δ*phz1/2* and Δ*phz1/2* Δ*nuoF* Δ*nqrF* strains over the course of 5 days, with zoom-ins on the initial 5 hours of current production. Curves are the average of 5 biological replicates. (D) Average PCN oxidation rate at the working electrode surface of Δ*phz1/2* cultures over days 1 to 5 of the anaerobic incubation. Each data point is the average of 5 biological replicates and error bars represent the 95% confidence interval. (E) Cell-specific metabolic rate of Δ*phz1/2* cells during days 1 to 5 of the anaerobic incubation across various concentrations of PCN. Each data point is the geometric mean of 5 biological replicates and error bars represent the 95% confidence interval.

MATERIALS AND METHODS

KEY RESOURCES TABLE

REAGENT or RESOURCE	**SOURCE**	**IDENTIFIER**
Bacterial and Virus Strains		
Pseudomonas aeruginosa UCBPP-PA14 Δ*phz1/2*	[80]Dietrich et al., 2006	N/A
P. aeruginosa UCBPP-PA14 Δ*phz1/2* Δ*nuoF* Δ*nqrF*	[47]Ciemniecki and Newman, 2023	N/A
P. aeruginosa UCBPP-PA14 Δ*phz1/2* Δ*ackA-pta*	[24]Glasser et al., 2014	N/A
P. aeruginosa UCBPP-PA14 Δ*phz1/2* Δ*nuoF* Δ*nqrF* Δ*ackA-pta*	This study	N/A
P. aeruginosa UCBPP-PA14 Δ*phz1/2* Δ*nuoF* Δ*nqrF*, *att*Tn7::*rhaP*$_{BAD}$-*nuoF*	This study	N/A
P. aeruginosa UCBPP-PA14 Δ*phz1/2* Δ*nuoF* Δ*nqrF*, *att*Tn7::*rhaP*$_{BAD}$-*nqrF*	This study	N/A
E. coli S17 (chemically competent for transformation)	ATCC	ATCC-BAA-2428
E. coli SM10/pTNS1 (chromosomal insertion helper strain)	[81]Choi and Schweizer, 2006	N/A
Chemicals, peptides, and recombinant proteins		
Difco LB Broth	BD	Cat#244620
Difco LB Agar	BD	Cat#244520
MOPS	Sigma-Aldrich	Cat#RDD003
Sodium Chloride	Fisher	Cat#BP358-212
Ammonium Chloride	Fisher	Cat#A649-500

Potassium Phosphate Monobasic	Fisher	Cat#P382-500
Magnesium Sulphate Heptahydrate	Fisher	Cat#M63-500
D-Glucose	Fisher	Cat#D16-500
Iron(II) Sulphate Heptahydrate	Fluka	Cat#44970
Phenazine-1-carboxamide	ChemScene	Cat#CS-W022931
Sodium Acetate Trihydrate	Fisher	Cat#S209-500
Potassium Nitrate	Fisher	Cat#P263-500
HADA	Tocris	Cat#6647
Propidium Iodide	Invitrogen	Cat#P1304MP
DCCD	Sigma-Aldrich	Cat#D80002
Colistin Sulfate Salt	Sigma-Aldrich	Cat#C4461
Ciprofloxacin	Abcam	Cat#ab141917
Ceftazidime Hydrate	Sigma-Aldrich	Cat#A6987
Tobramycin	Sigma-Aldrich	Cat#T4014
Oligonucleotides (5'-3')		
ackA-pta upstream forward: ACGACGGCCAGTGCCAAGCTTTCAGGCTGCAGAAGGACTG	This study	N/A
ackA-pta upstream reverse: GCCCACTGGGCGGCGTTCCTTCACTGCTCCTTGGTCTGCT	This study	N/A
ackA-pta downstream forward: AGCAGACCAAGGAGCAGTGAAGGAACCCCGCCCAGTGGGC	This study	N/A
ackA-pta downstream reverse: CATGATTACGAATTCGAGCTTACTGATCGCGGCCTGGAAGAAAAAGC	This study	N/A
Recombinant DNA		

pMQ30	[82]Shanks et al., 2006	N/A
pJM220	[83]Jeske and Altenbuchner, 2010	N/A
pMQ30 Δ*ackA-pta*	This study	N/A
pJM220 *rhaP*$_{BAD}$-*nuoF*	[47]Ciemniecki and Newman, 2023	N/A
pJM220 *rhaP*$_{BAD}$-*nqrF*	[47]Ciemniecki and Newman, 2023	N/A
Software and Algorithms		
GraphPad Prism 10 v10.1.1		https://www.graphpad.com/
ImageJ v2.0.0-rc-69/1.52p		https://imagej.net
OriginPro 2021		https://www.originlab.com

RESOURCE AVAILABILITY

Lead Contact

Further information and requests for resources and reagents should be directed to and will be fulfilled by the Lead Contact, Dianne Newman (dkn@caltech.edu).

Materials Availability

All bacterial strains are available upon request.

Data and Code Availability

Raw data are available upon request.

EXPERIMENTAL MODEL AND SUBJECT DETAILS

Bacterial growth conditions

All *Pseudomonas aeruginosa* UCBPP-PA14 strains were plated on LB agar from -80˚C glycerol stocks and grown overnight at 37˚C. Plates were stored at 4˚C for up to a week and were used to inoculate liquid cultures. Initial liquid cultures were grown in 7 mL of LB medium in glass culture tubes (VWR #47729-583) in an orbital shaker (New Brunswick, Innova 44) at 37˚C shaking at 250 rpm on a slant for 20 hours (final OD_{500nm} ~5).

Bacterial survival conditions in large electrochemical reactors

Initial cultures were used to inoculate a large 250 mL LB culture to an initial OD_{500nm} of 0.06. This large culture was grown under the same conditions as the initial culture for 5.5 hours to an OD_{500nm} of 3.0±0.2. These cells were pelleted (10 min, 6800 x*g*) and washed twice in a minimal medium (100 mM MOPS pH 7.2 with NaOH, 43 mM NaCl, 93 mM NH_4Cl, 3.7 mM KH_2PO_4, 1 mM $MgSO_4$), then resuspended to an OD of 75 and transferred into an MBraun nitrogen-only atmosphere glove box (Unilab model) containing the prepared glass reaction vessels (custom made) and held at 33˚C. 1 mL of the concentrated culture was then diluted into the main chamber of the large reaction vessels containing 99 mL of N_2-sparged minimal medium with 20 mM D-glucose and 3.6 µM $FeSO_4$ added (hereafter referred to as glucose minimal medium), along with 75 µM PCN in the relevant samples. This culture was connected to a potentiostat (Gamry Reference 600 model) via a graphite rod working electrode (Alfa Aesar #14738), platinum mesh counter electrode (custom-made using Alfa Aesar platinum gauze #10283), and $Ag/AgCl_{3M\ NaCl}$ reference electrode (Basi #MW-2030). The counter electrode was held in a small side-chamber separated from the main by a glass frit containing 9 mL minimal medium and 75 µM PCN. The working electrode was poised at a constant 0 mV vs. $Ag/AgCl_{3M\ NaCl}$ and the cultures were incubated with stirring using a stir rod in the vessel. 100 µL samples were removed periodically via a port over the main chamber of the vessel for CFU counting. All plastics used were left in the chamber to degas for at least three days before use.

Bacterial survival conditions in 96-potentiostat electrochemical plate

Initial cultures were pelleted and washed twice in minimal medium, resuspended to an OD of 75, and transferred into an anerobic Coy Chamber held at 33˚C and 2-3% H_2 containing the prepared 96-well electrochemical plate (custom-made as previously described[30]) with a screen-printed

carbon working electrode and counter electrode, and Ag/AgCl reference electrode. The culture was then diluted in N_2-sparged minimal medium to an OD of 15, and 10 µL of the concentrated culture was then diluted into each well of the plate containing 190 µL of N_2-sparged glucose minimal medium. The plate was sealed using both a slit-seal cover (BioChromato #R80.120.00) and an aluminum seal cover (DiversifiedBiotech #ALUM-1000) to prevent evaporation of the cultures between sampling. The plate was incubated at 33˚C without shaking in a custom 96-potentiostat system originally developed at the National Institute for Material Science, Japan. Every well's working electrode was held at a constant 0 mV vs. Ag/AgCl. Cyclic voltammograms measured with PCN as a standard showed that a potential +50 mV more positive was applied in the high-throughput reactor system than in the large reactor. On days 1, 3, and 5 of the incubation, the aluminum seal was removed and the well contents were mixed by pipetting a 150 µL volume. 10 µL was then removed for CFU dilution counting (20 µL on Day 5 to capture the lowest CFU concentrations). The plate was resealed with a fresh aluminum seal and then placed back in the 96-potentiostat system until the next CFU sampling. All plastics used were left in the chamber to degas for at least three days before use.

METHOD DETAILS

Mutant strain construction and complementation

All plasmids used in this work are listed in the Key Resources Table. Primers were synthesized by Integrated DNA Technologies and are also listed in the Key Resources Table. For all molecular cloning, plasmids were constructed using Gibson assembly reactions (NEB). Plasmids were chemically transformed into *E. coli* strain S17 and then conjugated into *P. aeruginosa* PA14. Mutants were constructed using standard homologous recombination using 1 kb regions flanking the gene(s) of interest in the pMQ30 plasmid. Genetic complement strains were constructed by reintroducing the deleted gene in *trans* at the *att*Tn7 site downstream of *glmS* in the *P. aeruginosa* genome using the pJM220 plasmid. For each complementation, the gene was designed to have its expression driven by a rhamnose-inducible promoter, and accordingly, complementation survival experiments were conducted using glucose minimal medium supplemented with L-rhamnose (0.005% w/v, 305 µM).

CFU counting

Phosphate buffered saline (PBS) was used for diluting cell cultures prior to plating for CFUs. Dilutions spanning 6-7 orders of magnitude were plated on LB agar using 5 µL spots and incubated at 37˚C overnight. Colonies were counted with the aid of a dissection microscope

(Nikon SMZ800). The furthest dilution spot containing at least 10 colonies was counted. Plates were kept for at least another 48 hours at room temp to check for delayed colony appearance; counts were updated when this rarely occurred. To accurately assess the degree of anaerobic killing caused by antibiotics, in that experiment (Figure 4C) samples for CFU counting were diluted anoxically in N_2-sparged PBS and plated on anoxic LB agar plates supplemented with 20 mM KNO_3. The plates were incubated at 37˚C anoxically for two days, then counted.

High-performance liquid chromatography

Samples were collected by centrifuging 1 mL of culture and passing the supernatant through a 0.22 µm filter. Samples were stored at -80˚C until analysis. Acetate was quantified using a Waters e2695 Separations Module equipped with a 2998 PDA Detector and run through an Aminex HPX-87H column (Bio-Rad) held at room temperature at a flow rate of 0.5 mL min^{-1} for 25 mins. The mobile phase used was 5 mM H_2SO_4. Retention time for acetate was validated with single species standards ranging from 0 to 20 mM, to calibrate peak area against a known concentration.

Cell dry weight measurements

On day 5 of the anaerobic survival in the large electrochemical reaction vessels, 2 mL samples of +PCN/pot culture were collected into pre-weighed tubes. The cultures were pelleted and resuspended twice in deionized water, then pelleted again. The supernatant was removed, and the pellet was dried overnight in a 55˚C drying oven. The dried pellets were then weighed on a microbalance, and the weight was divided by 2 * CFU / mL counts for that day to estimate the grams cell dry weight per cell.

Propidium iodide staining and imaging

Samples of culture from the large electrochemical reaction vessels were collected on day 5 of anaerobic incubation. The cells were pelleted and washed twice in anoxic PBS, then stained with 70 µM propidium iodide (Invitrogen) for 20 minutes in anoxic conditions. The cell suspension was then brought out of the MBraun chamber and spotted onto 1% (w/v) agar pads and imaged on a Nikon Eclipse Ti-2 inverted microscope using an ORCA-Flash4.0 V3 camera. Excitation light (555 nm) was supplied through a SpectraX LED light engine for a 200-ms exposure, and emission light was passed through a standard TRITC filter cube (Semrock) with the excitation filter removed. Identical LUTs were applied across all fluorescence images for comparison. The number of cells stained was counted manually with these LUTs applied using ImageJ's ROI manager; cell husks (those with no discernable phase-dark aspect) were excluded.

HADA single-cell growth measurements

250 mL LB cultures of cells were grown with 60 μM HADA label and washed as described in the *Experimental Model.* After the excess HADA was washed away the cells were inoculated into the anaerobic electrochemical reaction vessels as described above. For the nitrate control, smaller LB cell cultures containing HADA were used (7 mL) and washed identically before being inoculated into N_2-sparged balch tubes containing 10 mL of glucose minimal medium with 0.05% casamino acids and with or without 40 mM KNO_3 added. The balch tubes were incubated in the dark and at room temperature to ensure a slow growth over approximately the same time scale as the electrochemical survival experiment. On each day of either incubation (balch or echem), 0.5 mL of cells were sampled, pelleted, and resuspended in oxic PBS. On later days, the -PCN/pot samples were resuspended in smaller volumes of PBS to normalize cell density. 1 μL of the suspension was spotted onto 1% (w/v) agar pads and imaged on a Nikon microscope as described in *Propidium iodide staining and imaging*, using a 395 nm excitation, 200-ms exposure time, and a standard DAPI filter cube (Semrock) with the excitation filter removed. Due to global loss of fluorescence brightness at later timepoints, fluorescence LUTs were adjusted independently for each day to maximize visualization of cell body vs. pole staining. LUTs were set the same across images from the same day. The number of fluorescent poles vs. total poles was counted manually with these LUTs applied using ImageJ's ROI manager.

VBNC resuscitation

On days 3, 5 and 7 of the large reactor anaerobic incubation, samples of -PCN/pot culture from the vessels were pelleted and resuspended twice in oxic PBS of equal volume. A sample of this cell suspension was immediately plated for CFUs while another sample was diluted 1:10 in PBS in culture tubes and incubated at 33˚C aerobically without shaking. A sample of this aerobic resuscitation suspension was plated for CFUs after 1, 2, and 3 days of incubation.

ATP quantification assay

ATP was quantified using a Promega BacTiter-Glo kit according to the manufacturer's protocol. On day 7 of the large reactor anaerobic incubation, samples of culture from the vessels were pelleted and resuspended twice in anoxic PBS. Cells from the +PCN/pot condition were resuspended at a final concentration of 1x, while the -PCN/pot condition were resuspended at a 10x concentration to acquire sufficient luminescence from the assay. ATP quantification was divided by the CFUs for that day; resuscitated CFUs were used for the -PCN/pot condition.

Scanning electron microscopy

At the end of day 2 of the 96-potentiostat electrochemical plate survival experiment, after current had already subsided following the initial spike in the 375 μM PCN condition, samples were gently mixed by pipetting a 150 μL volume, then removed from the wells. 2.5% glutaraldehyde in PBS was added to each well and incubated for 10 min at 25˚C. The samples were carefully rinsed three times with PBS, then dehydrated by an ethanol wash gradient with 5 min incubations. The dehydrated samples were then washed with *t*-butanol twice for 5 minutes. The electrochemical board on the bottom of the plate was removed, and freeze-dried in *t*-butanol under vacuum for 2 days. The board was then platinum coated and observed by a Keyence VE-9800 scanning electron microscope at 10 or 20 kV.

QUANTIFICATION AND STATISTICAL ANALYSIS

To calculate an average PCN reduction rate in the 96-potentiostat system, current vs time traces were trimmed by 3 hrs immediately following the times when the plate was removed and returned to the potentiostat: these times following reconnection resulted in spurious, large spikes in current that settled back down to levels prior to removal of the plate. The current between days one and five was integrated, giving values with units nA*hr. This was then converted to units of electrons using standard conversion factors, divided by 90 hrs (4 d minus 6 hrs surrounding times of plate removal), divided by the geometric mean of the day 1-5 CFU $(0.2\ mL)^{-1}$ counts, and reported as units of electrons sec^{-1} $cell^{-1}$.

For all experiments, Prism 10 was used for analysis except for integration of current, which was done in OriginPro 2021. Technical replicates were averaged to generate single biological replicates before statistical analysis; therefore, all error ranges reported represent variation from biological replicates. Since CFUs were counted in log space, geometric means were used as a summary statistic. Any reported values that incorporated CFU counts (such as cell-specific metabolic rates) are also reported as a geometric mean. Otherwise, replicates were averaged using a linear mean.

SUPPLEMENTAL INFORMATION

Document S1. Figures S1-S4; Analysis of bacterial metabolic rate data from Hoehler et al. 2023, PNAS; $\Delta G^{\circ\prime}$ of PCN Facilitated Fermentation

Table S1. Excel file containing Hoehler et al. PNAS 2023 bacterial metabolic rates dataset with units transformed to electrons sec^{-1} $cell^{-1}$.

1

REFERENCES

1. Bergkessel, M., Basta, D.W., and Newman, D.K. (2016). The physiology of growth arrest: uniting molecular and environmental microbiology. Nat. Rev. Microbiol. *14*, 549–562. 10.1038/nrmicro.2016.107.

2. Morita, R.Y. (1988). Bioavailability of energy and its relationship to growth and starvation in nature. Can J Microbiol *34*, 436–441.

3. LaRowe, D.E., and Amend, J.P. (2015). Power limits for microbial life. Front. Microbiol. *6*, 718. 10.3389/fmicb.2015.00718.

4. Tijhuis, L., Van Loosdrecht, M.C., and Heijnen, J.J. (1993). A thermodynamically based correlation for maintenance gibbs energy requirements in aerobic and anaerobic chemotrophic growth. Biotechnol. Bioeng. *42*, 509–519. 10.1002/bit.260420415.

5. Hoehler, T.M., and Jørgensen, B.B. (2013). Microbial life under extreme energy limitation. Nat. Rev. Microbiol. *11*, 83–94. 10.1038/nrmicro2939.

6. Jin, X., Zhang, X., Ding, X., Tian, T., Tseng, C.-K., Luo, X., Chen, X., Lo, C.-J., Leake, M.C., and Bai, F. (2023). Sensitive bacterial Vm sensors revealed the excitability of bacterial Vm and its role in antibiotic tolerance. Proc Natl Acad Sci USA *120*, e2208348120. 10.1073/pnas.2208348120.

7. Lever, M.A., Rogers, K.L., Lloyd, K.G., Overmann, J., Schink, B., Thauer, R.K., Hoehler, T.M., and Jørgensen, B.B. (2015). Life under extreme energy limitation: a synthesis of laboratory- and field-based investigations. FEMS Microbiol. Rev. *39*, 688–728. 10.1093/femsre/fuv020.

8. Yin, L., Ma, H., Fones, E.M., Morris, D.R., and Harwood, C.S. (2023). ATP is a major determinant of phototrophic bacterial longevity in growth arrest. MBio *14*, e0360922. 10.1128/mbio.03609-22.

9. Robador, A., Amend, J.P., and Finkel, S.E. (2019). Nanocalorimetry Reveals the Growth Dynamics of *Escherichia coli* Cells Undergoing Adaptive Evolution during Long-Term Stationary Phase. Appl. Environ. Microbiol. *85*. 10.1128/AEM.00968-19.

10. Riedel, T.E., Berelson, W.M., Nealson, K.H., and Finkel, S.E. (2013). Oxygen consumption rates of bacteria under nutrient-limited conditions. Appl. Environ. Microbiol. *79*, 4921–4931. 10.1128/AEM.00756-13.

11. Stewart, P.S. (2015). Antimicrobial tolerance in biofilms. In Microbial Biofilms, pp. 269–285.

12. Thi, M.T.T., Wibowo, D., and Rehm, B.H.A. (2020). *Pseudomonas aeruginosa* Biofilms. Int. J. Mol. Sci. *21*. 10.3390/ijms21228671.

13. Levin-Reisman, I., Ronin, I., Gefen, O., Braniss, I., Shoresh, N., and Balaban, N.Q. (2017). Antibiotic tolerance facilitates the evolution of resistance. Science *355*, 826–830. 10.1126/science.aaj2191.

14. Stewart, P.S., and Costerton, J.W. (2001). Antibiotic resistance of bacteria in biofilms. Lancet *358*, 135–138. 10.1016/s0140-6736(01)05321-1.

15. Hall, C.W., and Mah, T.-F. (2017). Molecular mechanisms of biofilm-based antibiotic resistance and tolerance in pathogenic bacteria. FEMS Microbiol. Rev. *41*, 276–301. 10.1093/femsre/fux010.

16. Chiang, W.-C., Nilsson, M., Jensen, P.Ø., Høiby, N., Nielsen, T.E., Givskov, M., and Tolker-Nielsen, T. (2013). Extracellular DNA shields against aminoglycosides in *Pseudomonas aeruginosa* biofilms. Antimicrob. Agents Chemother. *57*, 2352–2361. 10.1128/AAC.00001-13.

17. Borriello, G., Werner, E., Roe, F., Kim, A.M., Ehrlich, G.D., and Stewart, P.S. (2004). Oxygen limitation contributes to antibiotic tolerance of *Pseudomonas aeruginosa* in biofilms. Antimicrob. Agents Chemother. *48*, 2659–2664. 10.1128/AAC.48.7.2659-2664.2004.

18. Mohr, K.I. (2016). History of antibiotics research. In Current Topics in Microbiology and Immunology, pp. 237–272.

19. Glasser, N.R., Saunders, S.H., and Newman, D.K. (2017). The colorful world of extracellular electron shuttles. Annu. Rev. Microbiol. *71*, 731–751. 10.1146/annurev-micro-090816-093913.

20. Schiessl, K.T., Hu, F., Jo, J., Nazia, S.Z., Wang, B., Price-Whelan, A., Min, W., and Dietrich, L.E.P. (2019). Phenazine production promotes antibiotic tolerance and metabolic heterogeneity in *Pseudomonas aeruginosa* biofilms. Nat. Commun. *10*, 762. 10.1038/s41467-019-08733-w.

21. VanDrisse, C.M., Lipsh-Sokolik, R., Khersonsky, O., Fleishman, S.J., and Newman, D.K. (2021). Computationally designed pyocyanin demethylase acts synergistically with tobramycin to kill recalcitrant *Pseudomonas aeruginosa* biofilms. Proc Natl Acad Sci USA *118*. 10.1073/pnas.2022012118.

22. Wang, Y., Kern, S.E., and Newman, D.K. (2010). Endogenous phenazine antibiotics promote anaerobic survival of *Pseudomonas aeruginosa* via extracellular electron transfer. J. Bacteriol. *192*, 365–369. 10.1128/JB.01188-09.

23. Eschbach, M., Schreiber, K., Trunk, K., Buer, J., Jahn, D., and Schobert, M. (2004). Long-term anaerobic survival of the opportunistic pathogen *Pseudomonas aeruginosa* via pyruvate fermentation. J. Bacteriol. *186*, 4596–4604. 10.1128/JB.186.14.4596-4604.2004.

24. Glasser, N.R., Kern, S.E., and Newman, D.K. (2014). Phenazine redox cycling enhances anaerobic survival in *Pseudomonas aeruginosa* by facilitating generation of ATP and a proton-motive force. Mol. Microbiol. *92*, 399–412. 10.1111/mmi.12566.

25. Hunt, K.A., Flynn, J.M., Naranjo, B., Shikhare, I.D., and Gralnick, J.A. (2010). Substrate-level phosphorylation is the primary source of energy conservation during anaerobic respiration of Shewanella oneidensis strain MR-1. J. Bacteriol. *192*, 3345–3351. 10.1128/JB.00090-10.

26. Benz, M., Schink, B., and Brune, A. (1998). Humic acid reduction by *Propionibacterium freudenreichii* and other fermenting bacteria. Appl. Environ. Microbiol. *64*, 4507–4512. 10.1128/AEM.64.11.4507-4512.1998.

27. Flynn, J.M., Ross, D.E., Hunt, K.A., Bond, D.R., and Gralnick, J.A. (2010). Enabling unbalanced fermentations by using engineered electrode-interfaced bacteria. MBio *1*. 10.1128/mBio.00190-10.

28. Tejedor-Sanz, S., Stevens, E.T., Li, S., Finnegan, P., Nelson, J., Knoesen, A., Light, S.H., Ajo-Franklin, C.M., and Marco, M.L. (2022). Extracellular electron transfer increases fermentation in lactic acid bacteria via a hybrid metabolism. eLife *11*. 10.7554/eLife.70684.

29. Okamoto, A., Tokunou, Y., Kalathil, S., and Hashimoto, K. (2017). Proton Transport in the Outer-Membrane Flavocytochrome Complex Limits the Rate of Extracellular Electron Transport. Angew. Chem. Int. Ed *56*, 9082–9086. 10.1002/anie.201704241.

30. Miran, W., Huang, W., Long, X., Imamura, G., and Okamoto, A. (2022). Multivariate landscapes constructed by Bayesian estimation over five hundred microbial electrochemical time profiles. Patterns (N Y) *3*, 100610. 10.1016/j.patter.2022.100610.

31. Wang, Y., and Newman, D.K. (2008). Redox reactions of phenazine antibiotics with ferric (hydr)oxides and molecular oxygen. Environ. Sci. Technol. *42*, 2380–2386. 10.1021/es702290a.

32. Jo, J., Price-Whelan, A., Cornell, W.C., and Dietrich, L.E.P. (2020). Interdependency of Respiratory Metabolism and Phenazine-Associated Physiology in *Pseudomonas aeruginosa* PA14. J. Bacteriol. *202*. 10.1128/JB.00700-19.

33. Saunders, S.H., Tse, E.C.M., Yates, M.D., Otero, F.J., Trammell, S.A., Stemp, E.D.A., Barton, J.K., Tender, L.M., and Newman, D.K. (2020). Extracellular DNA promotes efficient extracellular electron transfer by pyocyanin in *Pseudomonas aeruginosa* biofilms. Cell *182*, 919-932.e19. 10.1016/j.cell.2020.07.006.

34. Hoehler, T.M., Mankel, D.J., Girguis, P.R., McCollom, T.M., Kiang, N.Y., and Jørgensen, B.B. (2023). The metabolic rate of the biosphere and its components. Proc Natl Acad Sci USA *120*, e2303764120. 10.1073/pnas.2303764120.

35. Amy, P.S., and Morita, R.Y. (1983). Starvation-survival patterns of sixteen freshly isolated open-ocean bacteria. Appl. Environ. Microbiol. *45*, 1109–1115. 10.1128/aem.45.3.1109-1115.1983.

36. Bratbak, G., and Dundas, I. (1984). Bacterial dry matter content and biomass estimations. Appl. Environ. Microbiol. *48*, 755–757. 10.1128/aem.48.4.755-757.1984.

37. Chen, S.N. (2001). Growth Kinetics of *Pseudomonas aeruginosa*. Montana State University Masters Thesis. *https://scholarworks.montana.edu/xmlui/handle/1/8162*.

38. Geckil, H., Stark, B.C., and Webster, D.A. (2001). Cell growth and oxygen uptake of *Escherichia coli* and *Pseudomonas aeruginosa* are differently effected by the genetically engineered *Vitreoscilla* hemoglobin gene. J. Biotechnol. *85*, 57–66. 10.1016/s0168-1656(00)00384-9.

39. Finkel, S.E., and Kolter, R. (1999). Evolution of microbial diversity during prolonged starvation. Proc Natl Acad Sci USA *96*, 4023–4027. 10.1073/pnas.96.7.4023.

40. Yakhnina, A.A., McManus, H.R., and Bernhardt, T.G. (2015). The cell wall amidase AmiB is essential for *Pseudomonas aeruginosa* cell division, drug resistance and viability. Mol. Microbiol. *97*, 957–973. 10.1111/mmi.13077.

41. Navarro, P.P., Vettiger, A., Ananda, V.Y., Llopis, P.M., Allolio, C., Bernhardt, T.G., and Chao, L.H. (2022). Cell wall synthesis and remodelling dynamics determine division site architecture and cell shape in *Escherichia coli.* Nat. Microbiol. *7*, 1621–1634. 10.1038/s41564-022-01210-z.

42. Arai, H. (2011). Regulation and Function of Versatile Aerobic and Anaerobic Respiratory Metabolism in *Pseudomonas aeruginosa*. Front. Microbiol. *2*, 103. 10.3389/fmicb.2011.00103.

43. Pu, Y., Li, Y., Jin, X., Tian, T., Ma, Q., Zhao, Z., Lin, S.Y., Chen, Z., Li, B., Yao, G., et al. (2019). ATP-Dependent Dynamic Protein Aggregation Regulates Bacterial Dormancy Depth Critical for Antibiotic Tolerance. Mol. Cell *73*, 143-156.e4. 10.1016/j.molcel.2018.10.022.

44. Jiménez Otero, F., Newman, D.K., and Tender, L.M. (2023). Pyocyanin-dependent electrochemical inhibition of *Pseudomonas aeruginosa* biofilms is synergistic with antibiotic treatment. MBio *14*, e0070223. 10.1128/mbio.00702-23.

45. Schink, S., Ammar, C., Chang, Y.-F., Zimmer, R., and Basan, M. (2022). Analysis of proteome adaptation reveals a key role of the bacterial envelope in starvation survival. Mol. Syst. Biol. *18*, e11160. 10.15252/msb.202211160.

46. Schink, S., Polk, M., Athaide, E., Mukherjee, A., Ammar, C., Liu, X., Oh, S., Chang, Y.-F., and Basan, M. (2024). Survival dynamics of starving bacteria are determined by ion homeostasis that maintains plasmolysis. Nat. Phys. *20*, 1332–1338. 10.1038/s41567-024-02511-2.

47. Ciemniecki, J.A., and Newman, D.K. (2023). NADH dehydrogenases are the predominant phenazine reductases in the electron transport chain of *Pseudomonas aeruginosa.* Mol. Microbiol. *119*, 560–573. 10.1111/mmi.15049.

48. Torres, C.I., Marcus, A.K., Lee, H.-S., Parameswaran, P., Krajmalnik-Brown, R., and Rittmann, B.E. (2010). A kinetic perspective on extracellular electron transfer by anode-respiring bacteria. FEMS Microbiol. Rev. *34*, 3–17. 10.1111/j.1574-6976.2009.00191.x.

49. Imlay, J.A. (2013). The molecular mechanisms and physiological consequences of oxidative stress: lessons from a model bacterium. Nat. Rev. Microbiol. *11*, 443–454. 10.1038/nrmicro3032.

50. Glasser, N.R., Wang, B.X., Hoy, J.A., and Newman, D.K. (2017). The Pyruvate and α-Ketoglutarate Dehydrogenase Complexes of *Pseudomonas aeruginosa* Catalyze Pyocyanin and Phenazine-1-carboxylic Acid Reduction via the Subunit Dihydrolipoamide Dehydrogenase. J. Biol. Chem. *292*, 5593–5607. 10.1074/jbc.M116.772848.

51. Belliveau, N.M., Chure, G., Hueschen, C.L., Garcia, H.G., Kondev, J., Fisher, D.S., Theriot, J.A., and Phillips, R. (2021). Fundamental limits on the rate of bacterial growth and their influence on proteomic composition. Cell Syst. *12*, 924-944.e2. 10.1016/j.cels.2021.06.002.

52. Basan, M., Honda, T., Christodoulou, D., Hörl, M., Chang, Y.-F., Leoncini, E., Mukherjee, A., Okano, H., Taylor, B.R., Silverman, J.M., et al. (2020). A universal trade-off between growth and lag in fluctuating environments. Nature *584*, 470–474. 10.1038/s41586-020-2505-4.

53. Hoehler, T.M., Amend, J.P., Jørgensen, B.B., Orphan, V.J., and Lever, M.A. (2024). Editorial: Studies on life at the energetic edge – from laboratory experiments to field-based investigations, volume II. Front. Microbiol. *14*. 10.3389/fmicb.2023.1351761.

54. Røy, H., Kallmeyer, J., Adhikari, R.R., Pockalny, R., Jørgensen, B.B., and D'Hondt, S. (2012). Aerobic microbial respiration in 86-million-year-old deep-sea red clay. Science *336*, 922–925. 10.1126/science.1219424.

55. Jaussi, M., Jørgensen, B.B., Kjeldsen, K.U., Lomstein, B.A., Pearce, C., Seidenkantz, M.-S., and Røy, H. (2023). Cell-specific rates of sulfate reduction and fermentation in the sub-seafloor biosphere. Front. Microbiol. *14*, 1198664. 10.3389/fmicb.2023.1198664.

56. Kanaan, G., Hoehler, T.M., Iwahana, G., and Deming, J.W. (2023). Modeled energetics of bacterial communities in ancient subzero brines. Front. Microbiol. *14*, 1206641. 10.3389/fmicb.2023.1206641.

57. Makarieva, A.M., Gorshkov, V.G., Li, B.-L., Chown, S.L., Reich, P.B., and Gavrilov, V.M. (2008). Mean mass-specific metabolic rates are strikingly similar across life's major domains: Evidence for life's metabolic optimum. Proc Natl Acad Sci USA *105*, 16994–16999. 10.1073/pnas.0802148105.

58. Price, P.B., and Sowers, T. (2004). Temperature dependence of metabolic rates for microbial growth, maintenance, and survival. Proc Natl Acad Sci USA *101*, 4631–4636. 10.1073/pnas.0400522101.

59. Stouthamer, A.H. (1973). A theoretical study on the amount of ATP required for synthesis of microbial cell material. Antonie Van Leeuwenhoek *39*, 545–565.

60. Mccollom, T.M., and Amend, J.P. (2005). A thermodynamic assessment of energy requirements for biomass synthesis by chemolithoautotrophic micro-organisms in oxic and anoxic environments. Geobiology *3*, 135–144. 10.1111/j.1472-4669.2005.00045.x.

61. van Bodegom, P. (2007). Microbial maintenance: a critical review on its quantification. Microb. Ecol. *53*, 513–523. 10.1007/s00248-006-9049-5.

62. Walker, R.M., Sanabria, V.C., and Youk, H. (2023). Microbial life in slow and stopped lanes. Trends Microbiol. 10.1016/j.tim.2023.11.014.

63. Koch, A.L. (1971). The Adaptive Responses of *Escherichia coli* to a Feast and Famine Existence. Adv Microb Physiol *6*, 147–217.

64. Rothman, D.H. (2024). Slow closure of Earth's carbon cycle. Proc Natl Acad Sci USA *121*, e2310998121. 10.1073/pnas.2310998121.

65. Basta, D.W., Bergkessel, M., and Newman, D.K. (2017). Identification of fitness determinants during energy-limited growth arrest in *Pseudomonas aeruginosa*. MBio *8*, e01170-17. 10.1128/mBio.01170-17.

66. Kaila, V.R.I., and Wikström, M. (2021). Architecture of bacterial respiratory chains. Nat. Rev. Microbiol. *19*, 319–330. 10.1038/s41579-020-00486-4.

67. Raba, D.A., Rosas-Lemus, M., Menzer, W.M., Li, C., Fang, X., Liang, P., Tuz, K., Minh, D.D.L., and Juárez, O. (2018). Characterization of the *Pseudomonas aeruginosa* NQR complex, a bacterial proton pump with roles in autopoisoning resistance. J. Biol. Chem. *293*, 15664–15677. 10.1074/jbc.RA118.003194.

68. Schink, B. (1997). Energetics of syntrophic cooperation in methanogenic degradation. Microbiol. Mol. Biol. Rev. *61*, 262–280. 10.1128/mmbr.61.2.262-280.1997.

69. Jackson, B.E., and McInerney, M.J. (2002). Anaerobic microbial metabolism can proceed close to thermodynamic limits. Nature *415*, 454–456. 10.1038/415454a.

70. Caro, T.A., McFarlin, J., Jech, S., Fierer, N., and Kopf, S. (2023). Hydrogen stable isotope probing of lipids demonstrates slow rates of microbial growth in soil. Proc Natl Acad Sci USA *120*, e2211625120. 10.1073/pnas.2211625120.

71. Coskun, Ö.K., Özen, V., Wankel, S.D., and Orsi, W.D. (2019). Quantifying population-specific growth in benthic bacterial communities under low oxygen using $H_2{}^{18}O$. ISME J. *13*, 1546–1559. 10.1038/s41396-019-0373-4.

72. Blazewicz, S.J., Hungate, B.A., Koch, B.J., Nuccio, E.E., Morrissey, E., Brodie, E.L., Schwartz, E., Pett-Ridge, J., and Firestone, M.K. (2020). Taxon-specific microbial growth and mortality patterns reveal distinct temporal population responses to rewetting in a California grassland soil. ISME J. *14*, 1520–1532. 10.1038/s41396-020-0617-3.

73. Kirchman, D.L. (2016). Growth rates of microbes in the oceans. Ann. Rev. Mar. Sci. *8*, 285–309. 10.1146/annurev-marine-122414-033938.

74. Jaishankar, J., and Srivastava, P. (2017). Molecular basis of stationary phase survival and applications. Front. Microbiol. *8*, 2000. 10.3389/fmicb.2017.02000.

75. Jones, E.M., Marken, J.P., and Silver, P.A. (2024). Synthetic microbiology in sustainability applications. Nat. Rev. Microbiol. 10.1038/s41579-023-01007-9.

76. Shi, Z., Crowell, S., Luo, Y., and Moore, B. (2018). Model structures amplify uncertainty in predicted soil carbon responses to climate change. Nat. Commun. *9*, 2171. 10.1038/s41467-018-04526-9.

77. Liang, C., Schimel, J.P., and Jastrow, J.D. (2017). The importance of anabolism in microbial control over soil carbon storage. Nat. Microbiol. *2*, 17105. 10.1038/nmicrobiol.2017.105.

78. Dietrich, L.E.P., Okegbe, C., Price-Whelan, A., Sakhtah, H., Hunter, R.C., and Newman, D.K. (2013). Bacterial community morphogenesis is intimately linked to the intracellular redox state. J. Bacteriol. *195*, 1371–1380. 10.1128/JB.02273-12.

79. Babin, B.M., Atangcho, L., van Eldijk, M.B., Sweredoski, M.J., Moradian, A., Hess, S., Tolker-Nielsen, T., Newman, D.K., and Tirrell, D.A. (2017). Selective Proteomic Analysis of Antibiotic-Tolerant Cellular Subpopulations in *Pseudomonas aeruginosa* Biofilms. MBio *8*. 10.1128/mBio.01593-17.

80. Dietrich, L.E., Price-Whelan, A., Petersen, A., Whiteley, M., and Newman, D.K. (2006). The phenazine pyocyanin is a terminal signalling factor in the quorum sensing network of *Pseudomonas aeruginosa*. Mol. Microbiol. *61*, 1308–1321. 10.1111/j.1365-2958.2006.05306.x.

81. Choi, K.-H., and Schweizer, H.P. (2006). mini-Tn7 insertion in bacteria with single *att*Tn7 sites: example *Pseudomonas aeruginosa*. Nat. Protoc. *1*, 153–161. 10.1038/nprot.2006.24.

82. Shanks, R.M.Q., Caiazza, N.C., Hinsa, S.M., Toutain, C.M., and O'Toole, G.A. (2006). *Saccharomyces cerevisiae*-based molecular tool kit for manipulation of genes from gram-negative bacteria. Appl. Environ. Microbiol. *72*, 5027–5036. 10.1128/AEM.00682-06.

83. Jeske, M., and Altenbuchner, J. (2010). The *Escherichia coli* rhamnose promoter $rhaP_{BAD}$ is in *Pseudomonas putida* KT2440 independent of Crp–cAMP activation. Appl. Microbiol. Biotechnol. *85*, 1923–1933. 10.1007/s00253-009-2245-8.